JCTC Journal of Chemical Theory and Computation

# Exploring Multidimensional Free Energy Landscapes Using Time-Dependent Biases on Collective Variables

Jérome Hénin,*[,†,||] Giacomo Fiorin,[‡] Christophe Chipot,[§,⊥] and Michael L. Klein[‡]

*Center for Molecular Modeling, Department of Chemistry, University of Pennsylvania, Philadelphia, Pennsylvania 19104, Institute for Computational Molecular Science and Department of Chemistry, Temple University, Philadelphia, Pennsylvania 19122, and Department of Physics and Beckman Institute for Advanced Science and Engineering, University of Illinois at Urbana−Champaign, Urbana, Illinois 61820*

Received August 18, 2009

**Abstract:** A new implementation of the adaptive biasing force (ABF) method is described. This implementation supports a wide range of collective variables and can be applied to the computation of multidimensional energy profiles. It is provided to the community as part of a code that implements several analogous methods, including metadynamics. ABF and metadynamics have not previously been tested side by side on identical systems. Here, numerical tests are carried out on processes including conformational changes in model peptides and translocation of a halide ion across a lipid membrane through a peptide nanotube. On the basis of these examples, we discuss similarities and differences between the ABF and metadynamics schemes. Both approaches provide enhanced sampling and free energy profiles in quantitative agreement with each other in different applications. The method of choice depends on the dimension of the reaction coordinate space, the height of the barriers, and the relaxation times of degrees of freedom in the orthogonal space, which are not explicitly described by the chosen collective variables.

## Introduction

A variety of approaches for accelerated sampling and mapping of free energy landscapes from molecular simulations have been proposed over the years (see refs 1–3 for reviews). Typically, these approaches have only been used by a limited number of groups that specialize in theory and method development. Only rarely have such methods been made readily available to the broad computational chemistry and biophysics community, as this requires well-documented implementations compatible with the standard tools of this community: parallel simulation programs capable of high-throughput, large-scale calculations. An implementation of the metadynamics approach of Laio and Parrinello[4] for mainstream simulation packages has been made available only very recently.[5]

The previous publicly available implementation[6] of the adaptive biasing force method[7,8] (ABF), in version 2.6 of NAMD,[9] has been applied successfully to a number of challenging cases. The domains of application of ABF include the recognition and association of peptides or proteins,[10–12] peptide− or protein−lipid interactions,[13–15] small molecules interacting in a confined environment,[16] cyclodextrin association with cholesterol,[17] steroid drugs,[18] and molecular ions,[19] as well as cyclodextrin self-assembly.[20] Translocation of molecules or ions through natural, transmembrane channel proteins[21–24] and transporters,[25] through synthetic pores,[26] and across simple liquid interfaces[27] have also been studied. Another class of applications involves conformational changes in peptides,[28,29] proteins,[30–32] and

* Corresponding author e-mail: jhenin@ifr88.cnrs-mrs.fr.
† University of Pennsylvania.
‡ Temple University.
§ University of Illinois at Urbana−Champaign.
|| Current address: Laboratoire d'Ingénierie des Systèmes Macromoléculaires, CNRS UPR9027, Marseille, France.
⊥ On leave from Equipe de Dynamique des Assemblages Membranaires, UMR CNRS/UHP 7565, Nancy Université BP 239, Nancy, France.

10.1021/ct9004432 
Published on Web 12/03/2009

nucleic acids.[33] Despite the number and variety of such applications, that implementation carried significant technical limitations, particularly its restriction to one-dimensional free energy profiles.

When a low-dimension reduced representation comprised of a few degrees of freedom is used to describe a complex process, hidden barriers orthogonal to the chosen parameters are likely to exist. The orthogonal space random walk strategy[34,35] has been proposed by Zheng et al. as a means of overcoming such hidden barriers. While a promising idea, likely to be further explored and built upon in the future, it treats the orthogonal space using a single degree of freedom, which may or may not suffice to overcome hidden barriers effectively in complex examples; in many instances, a well-chosen degree of freedom may well yield better results. Still, the orthogonal space random walk approach has the advantage of generality, as it extends a predefined reaction coordinate space without requiring any additional physical insight into the particular process being examined.

Using collective variables well-adapted to the chemical or biophysical process under scrutiny is critical, and specific problems frequently require tailored variables. We recently developed a new code, the Collective Variables Module, for version 2.7 of the high-performance simulation program NAMD. This code supports a large set of commonly employed variables, offers the possibility to use polynomial combinations of such variables, and can be readily adapted to deal with atypical problems; the full list of features and technical details will be discussed elsewhere. In this contribution, we illustrate its most important application, that is, sampling multidimensional collective variable space and reconstructing free energy landscapes. Example simulations are presented, which make use of the first publicly released ABF implementation capable of multidimensional calculations, and are discussed alongside the results of identical simulations performed with the metadynamics method.[4]

In the following section, the theoretical framework underlying this ABF implementation is described, and its range of applicability as well as its technical limitations are discussed. Next, physical processes in four molecular systems are explored using ABF, conformational equilibria of *N*-acetyl-*N*′-methylalaninamide (NANMA), Met-enkephalin, and deca-alanine, as well as ion diffusion through a membrane-spanning peptide nanotube. The metadynamics approach is also applied to the NANMA and nanotube examples. The deca-alanine case is used to document the application of ABF to a three-dimensional reaction coordinate. The choice of reaction coordinate space, numerical behavior, and convergence of the simulations, as well as compared properties of the two methods, are discussed.

## Methods

**Defining Reaction Coordinates.** The strategy described here consists of using ABF or metadynamics to map a complex, slow molecular process, based on simulated trajectories that are orders of magnitude shorter than its natural time scale. This can be achieved by navigating a carefully chosen reduced representation, the "reaction coordinate space", in an accelerated fashion. The minimum requirement for this approach to be useful is that the reduced representation resolves the end points of the transformation and, more generally, all states that one wishes to describe based on empirical knowledge of the system. For numerical efficiency of the sampling scheme, however, the chosen degrees of freedom should capture all kinetically significant regions of configuration space: the metastable intermediates and most probable transition pathways.

In chemical terminology, a reaction coordinate is a one-dimensional geometric parameter that can be used to measure the progression of a reaction.[36] Moving from the realm of chemical reactions to that of physical transformations in soft matter and biological systems, however, fluctuations along many degrees of freedom may become as important to the reaction kinetics as the progression along any particular pathway. One-dimensional descriptors then become less useful, while constructing single variables that may play this role becomes more cumbersome and less intuitive.

For the purpose of numerical simulations, the optimal situation is to achieve time scale separation, whereby all key slow degrees of freedom are described explicitly, so that other degrees of freedom coupled to the transformation relax on a short time scale, as compared to the length of the simulated trajectories. This time scale influences both the diffusion rate of the system in reaction coordinate space and the rate of convergence of quantities that are measured as a function of the reaction coordinates, such as the free energy gradient in ABF calculations.

**Thermodynamic Integration in Configuration Space.** This section gives a brief historical overview of the theoretical results that led to the ABF method.[7] The general principles of thermodynamic integration (TI) can be found in early work by Kirkwood[37] and Zwanzig.[38] In TI, the free energy derivative is computed as the ensemble average of an instantaneous force, $F$, acting on the reaction parameter $\xi$:

$$\frac{\mathrm{d}A}{\mathrm{d}\xi} = -\langle F \rangle_{\xi} \tag{1}$$

In most applications of TI to configurational variables, sampling along the reaction pathway is obtained by constraining the reaction coordinate, the so-called "blue moon ensemble". In one of the earliest cases, $F$ was simply obtained as the force exerted by the solvent on two atomic ions, projected onto the interionic distance.[39] Shortly afterward, a general expression for the average force was proposed by Carter et al.[40] The expression features a Jacobian correction term, purely geometric in origin, and is based on an explicit set of generalized coordinates $(\xi, \mathbf{q})$ including the reaction coordinate $\xi$:

$$F(\xi, \mathbf{q}) = -\frac{\partial U(\xi, \mathbf{q})}{\partial \xi} + k_{\mathrm{B}}T\frac{\partial \ln|J(\xi, \mathbf{q})|}{\partial \xi} \tag{2}$$

The explicit coordinate transform from $(x_i)$ to $(\xi, \mathbf{q})$ is needed to define and compute both the Jacobian determinant $|J(\xi, \mathbf{q})|$ and the partial derivative $\partial U(\xi, \mathbf{q})/\partial \xi$ of the potential energy $U$. The latter quantity depends implicitly on the vector field $(\partial x_i/\partial \xi)$, hereafter referred to as "inverse gradient". This vector field can be thought of as the direction along which

an infinitesimal change in $\xi$ is propagated in Cartesian coordinates, the complementary coordinates $\mathbf{q}$ being kept constant. By definition, at any point of configuration space, the dot product of the inverse gradient with the Cartesian gradient of $\xi$ is unity.

A significant step toward lifting the requirement of a full coordinate transform was accomplished by Ruiz-Montero et al.,[41] who proposed to use an implicit set of complementary coordinates $\mathbf{q} \equiv (q_i)$ that would obey:

$$\nabla q_i \cdot \nabla q_j = \delta_{ij} \tag{3}$$

$$\nabla \xi \cdot \nabla q_i = 0 \tag{4}$$

Under these assumptions, a simpler expression holds:

$$F(\xi, \mathbf{q}) = -\frac{\nabla U \cdot \nabla \xi}{|\nabla \xi|^2} + k_B T \frac{(\nabla |\nabla \xi|) \cdot \nabla \xi}{|\nabla \xi|^3} \tag{5}$$

In this formulation, the inverse gradient is replaced with a vector proportional to the gradient $\nabla\xi$, and no generalized coordinate other than $\xi$ itself is involved. Den Otter and Briels noted,[42] however, that a set of complementary coordinates obeying eqs 3 and 4 is not guaranteed to exist and showed that, in fact, it does not exist in a case as simple as polar coordinates in two dimensions.

In a later publication,[43] den Otter put forward the visionary idea that the change in $\xi$ can be propagated along an arbitrary vector field, provided that it satisfies orthonormality conditions similar to eqs 3 and 4. This obviates the need for a full coordinate transform, and the propagating field generalizes the role played by the inverse gradient (which is always a possible choice if a coordinate transform is available). Ciccotti, Kapral, and Vanden-Eijnden[44] extended den Otter's formalism to a multidimensional reaction coordinate $\boldsymbol{\xi} = (\xi_i)$, in the presence of a set of constraints of the form $\sigma_k(\mathbf{x}) = 0$. For each coordinate $\xi_i$, let $\mathbf{v}_i$ be a vector field ($\mathbb{R}^{3N} \rightarrow \mathbb{R}^{3N}$, where $N$ is the number of atoms) satisfying, for all $j$ and $k$:

$$\mathbf{v}_i \cdot \nabla \xi_j = \delta_{ij} \tag{6}$$

$$\mathbf{v}_i \cdot \nabla \sigma_k = 0 \tag{7}$$

The $i$th partial derivative of the free energy surface can then be calculated as the ensemble average of the following thermodynamic force:

$$F_i(\boldsymbol{\xi}, \mathbf{q}) = -\nabla U \cdot \mathbf{v}_i + k_B T \nabla \cdot \mathbf{v}_i \tag{8}$$

Ciccotti et al. note that a set of vector fields $\mathbf{v}_i$ can always be constructed by orthonormalization. There is, however, no simple algorithm to evaluate the divergence of $\mathbf{v}_i$ numerically. This term involves the second spatial derivatives of $(\xi_i)$, making numerical schemes potentially costly and subject to high variance. In practice, analytical derivation is often possible, although cumbersome; the present implementation relies on such analytical derivatives.

**Adaptive Biasing Force Method for Multidimensional Coordinates.** The ABF method was put forth in 2001 by Darve and Pohorille.[7] Its principle is to perform thermodynamic integration in configuration space based on an unconstrained simulation, in which a history-dependent bias is applied; this bias is designed to cancel the running estimate of the local free energy gradient. In the same contribution, an estimator making use of a constraint algorithm was proposed. More recently, the same authors have described a new estimator for the free energy gradient, based on time derivatives of the reaction coordinates, and its use for multidimensional ABF calculations.[8]

The NAMD 2.6 implementation of the ABF method using eqs 2 and 8 (in the original one-dimensional version of den Otter) has been described previously.[6] In comparison, the present implementation offers a greatly extended range of applications by allowing multidimensional free energy surfaces to be computed, and by handling linear combinations of predefined variables. Multidimensional ABF may be implemented on the basis of various formulations of thermodynamic integration: this implementation relies on computation of free energy gradients based on eq 8, in arbitrary dimension, as published by Ciccotti et al.[44] The algorithm is otherwise identical to that described previously.[6–8] Much of the new code base is shared with the rest of the Collective Variables Module, which will be described in detail elsewhere. Increased flexibility does imply some restrictions on the way variables can be combined: as in the previous implementation, eq 7 has to be satisfied, should any degree of freedom be constrained. In addition, collective variables must obey eq 6. For modularity, program objects handling different collective variables function independently. As a result, the option of run-time orthogonalization suggested by Ciccotti et al.[44] is not available, and the orthogonality relationship 6 has to be enforced by construction of the variables. A trivial way of achieving this is to combine variables that depend on nonoverlapping sets of Cartesian coordinates, as illustrated by most of the ABF calculations discussed in the following sections. In the case of chloride permeation through the nanotube, the longitudinal and radial coordinates are orthogonal by construction.

The direct benefit of an ABF simulation, besides enhanced sampling in the molecular dynamics (MD) trajectory, is an estimate of the free energy gradient, discretized on a regular lattice. In dimensions higher than one, several numerical routes can be followed to integrate this gradient and obtain the free energy surface itself. Other groups have proposed[8,45] to expand the free energy on a basis of spline or Gaussian functions and minimize the square deviation of the gradient at a predefined set of control points. Here, a different approach is adopted: the free energy landscape is reconstructed on the basis of discrete Monte Carlo sampling of the lattice. Convergence is accelerated by introducing a history-dependent biasing potential, which is incremented locally at each step, much in the spirit of conformational flooding[46] or metadynamics.[4] This method has fewer tunable parameters than the aforementioned techniques, and it is natural to use the same lattice that was used to discretize the ABF calculation. Unlike the method based on smooth radial functions,[45] its convergence speed worsens rapidly as the dimension increases. ABF calculations, however, are unlikely to be performed in high dimension due to the computational obstacles that the current form of the algorithm entails. Indeed, only one ABF result in dimension higher than one has been reported so far,[8] that is, the two-dimensional Ramachandran map of NANMA. It is, nevertheless, conceivable that ABF

could be recast into a more scalable form, paving the way for higher-dimension applications.

## Computational Details

**Molecular Dynamics Simulations.** All simulations reported here were carried out using version 2.7b1 of the molecular dynamics program NAMD.[9,47] Condensed-phase simulations were performed in the isobaric−isothermal ensemble. The pressure and the temperature were fixed at 1 bar and 300 K, respectively, employing the Langevin piston algorithm[48] and softly damped Langevin dynamics. Periodic boundary conditions were applied in the three directions of Cartesian space. Short-range Lennard-Jones and Coulomb interactions were truncated smoothly by means of a 12 Å spherical cutoff with a switching function applied beyond 10 Å. The particle-mesh Ewald method[49] was employed to compute long-range electrostatic interactions. The Verlet I *r*-RESPA multiple time-step integrator[50] was used with a time step of 2 and 4 fs for for updating short- and long-range forces, respectively. Covalent bonds involving a hydrogen atom were constrained to their equilibrium length. Gas-phase simulations were performed using a 0.5 fs time step, which is appropriate to ensure energy conservation, and bond lengths were not constrained. Other parameters were similar to those of condensed-phase simulations. The different chemical systems described in the present contribution were described by the all-atom CHARMM force field,[51] supplemented by the TIP3P water model.[52]

**Free Energy Calculations.** The present results were obtained using a software framework known as Collective Variables Module and implemented in NAMD, versions 2.7b1 and following. Detailed user-oriented documentation is available;[47] technical details will be published elsewhere.

*Conformational Equilibrium of N-acetyl-N′-methylalaninamide.* The first application consists of a proof-of-concept simulation of the prototypical, terminally blocked amino acid *N*-acetyl-*N*′-methylalaninamide (NANMA), often referred to as "alanine dipeptide".[53] Conformational sampling was performed in vacuum. The $\phi$ and $\psi$ torsional angles of the backbone were handled as coupled variables covering each the full, [−180°; +180°] range of the Ramachandran free energy map.[54] To increase the efficiency of the calculation, the latter map was split into four individual quadrants, corresponding to fully independent simulations. Each quadrant was discretized into bins 2.5° × 2.5° wide, in which the force acting along the collective variables was accrued. In each quadrant, 25 ns of sampling was collected. A threshold of 100 force samples was set prior to application of the adaptive biasing force. Reconstruction of the complete free energy landscape was achieved by numerical integration of the two-dimensional gradients. The Ramachandran map was also sampled by means of the metadynamics algorithm. Sampling was collected from a 30 ns trajectory, and Gaussian biasing potentials of width 10° and height 0.1 kcal/mol were accumulated every 500 fs. The free energy difference between the $C_{7eq}$ and $C_{7ax}$ states was computed by integration over the corresponding regions $V$ and $V'$ of $(\phi, \psi)$-space according to:

$$e^{-\beta\Delta A} = \frac{\int_V e^{-\beta\Delta A(\phi,\psi)}\, d\phi\, d\psi}{\int_{V'} e^{-\beta\Delta A(\phi,\psi)}\, d\phi\, d\psi} \quad (9)$$

Transition between the two lowest free energy states of the Ramachandran map, that is, $C_{7eq}$ and $C_{7ax}$, which are stabilized by an intramolecular hydrogen bond formed between the carbonyl moiety of one terminus and the amino moiety of the other, was investigated with one-dimensional ABF, using as a collective variable the difference between two distance root mean-square deviations, $\xi = \mathrm{rmsd}(C_{7eq}) - \mathrm{rmsd}(C_{7ax})$. To ensure orthogonality of the variables according to eq 6, the two RMSDs were defined as two distinct subsets formed of six atoms of the peptide chain. Three independent, 20, 20, and 40 ns long, simulations were run, using a threshold of 5000 force samples prior to applying the adaptive biasing force along the chosen degrees of freedom.

*Chloride Ion Permeation across a Peptide Nanotube.* In this second application, translocation of an halide ion through a chemically engineered tubular structure is examined. Peptide nanotubes, which can be viewed as tailored synthetic ion channels, result from the self-assembly of cyclic peptides formed by alternated D-L-α-amino acids,[55,56] by means of a network of intermolecular hydrogen bonds.[57]

The peptide nanotube considered here consisted of eight stacked *cyclo*[LW]$_4$ units, where underlined letters denote D-amino acids, immersed in a thermalized palmitoyl-oleoyl-phosphatidylcholine (POPC) bilayer formed by 48 lipid units, in equilibrium with 1572 water molecules. The complete molecular assembly was placed in a simulation cell of initial dimensions equal to 36 × 41 × 79 Å$^3$. The two-dimensional free energy landscape delineating the translocation of a chloride ion across the tubular structure was determined along the longitudinal, $\zeta$, and the radial, $\rho$, directions of the latter. Specifically, the model reaction coordinate was chosen as a subset of cylindrical polar coordinates: the distance separating the ion from the center of mass of the peptide nanotube, projected onto its long axis, in conjunction with the distance separating the ion from the axis. The reaction path spanned 40 and 3 Å in the $\zeta$- and in the $\rho$-directions, respectively. In the ABF calculation, force samples were accrued in bins 0.1 Å wide. To increase the efficiency of the calculation, it was stratified into four nonoverlapping windows extending over 10 Å each in the $\zeta$-direction and in which individual 30 ns trajectories were generated, corresponding to a total simulation time of 120 ns. A metadynamics simulation was performed using the same pair of variables, similarly split into four windows along $z$. Gaussian hills of width 0.3 Å and height 0.1 kcal/mol were added every 200 fs; the calculation was run for 44 ns.

*Structure of Met-enkephalin in an Aqueous Solution.* In this third application, a set of collective variables is utilized to explore the possible conformations of the short peptide Met-enkephalin in an explicit solvent. Met-enkephalin is an endogenous opioid, five-residue neurotransmitter peptide, YGGFM, found in mammals and known to inhibit the release of neurotransmitters upon activation of the relevant opioid receptors. On account of its small size and biological relevance, it has served as a paradigmatic system for

conformational search based on a variety of computational approaches.[58–72]

The molecular system consisted of Met-enkephalin immersed in a bath of 778 water molecules, which corresponds to a simulation cell of initial dimensions equal to 29 × 29 × 29 Å$^3$. Conformational search was conducted in a two-dimensional space, combining the radius of gyration ($R_g$) of the short peptide to its distance rmsd with respect to a reference, helical structure. The reaction path spanned, respectively, 3.5 and 4.0 Å, in the $R_g$ and rmsd directions. To ensure that the force measured along one variable does not act on the other (eq 6), two distinct subsets of atoms were defined to compute the distance rmsd and the radius of gyration, the five α-carbon atoms and all other heavy atoms of the peptide chain, respectively. The instantaneous force was accrued in bins 0.05 Å wide. No adaptive biasing force was applied below a threshold of 200 samples. The limited range covered by the two variables obviated the need for a stratification strategy. The two-dimensional free energy landscape reported in the present contribution was obtained from a total simulation time of 80 ns.

*Conformational Landscape of Deca-alanine.* To explore metastable conformations of deca-alanine in vacuum, starting points were chosen manually from preliminary ABF trajectories, and used as the seed for unbiased, 30 ns simulations, where relaxation and possible transitions to other local minima were monitored. Conformations typical of the long-lived, metastable conformers were extracted from these unbiased trajectories. The conformational free energy landscape of the peptide was then explored by means of ABF-biased simulations in one, two, and three dimensions. The one-dimensional calculation was based on the end-to-end distance $d$, that is, the distance between the carbonyl carbon atoms of residues 1 and 10. The duration of the simulated trajectory was 500 ns. The two-dimensional, 200 ns ABF calculation was based on both $d$ and the minimal rmsd between the current structure and a typical $\beta$-hairpin conformation (structure E in Figure 6). The rmsd was calculated using α-carbon atoms only. Finally, a 400 ns three-dimensional ABF simulation was carried out: the set of collective variables was composed of three RMSDs, with respect to the typical α-helical, turn/$3_{10}$-helix, and $\omega$-shaped turn, respectively. The structures of these conformers are described in the Results section. The three RMSDs were defined on the basis of α-carbon, carbonyl carbon, and peptide nitrogen atoms, respectively; these nonoverlapping sets of atoms ensured that eq 6 was obeyed.

## Results and Discussion

**Conformational Equilibrium of *N*-Acetyl-*N*′-methylalaninamide.** In the past 30 years, the conformational equilibrium of NANMA has been investigated in ample detail, employing a variety of numerical approaches and potential energy functions.[4,8,53,73–93] Accurate reproduction of the gas-phase, two-dimensional Ramachandran free energy map, therefore, hardly constitutes a methodological prowess. Popular, well-established approaches like umbrella sampling[94] used in conjunction with the weighted histogram analysis method[95] have proven to be perfectly adapted to rank with the desired accuracy the conformational states accessible to this paradigmatic peptide.[82] Furthermore, in several instances, NANMA has served as a discriminating test case for assessing the performance of novel numerical schemes.[8,83,96]

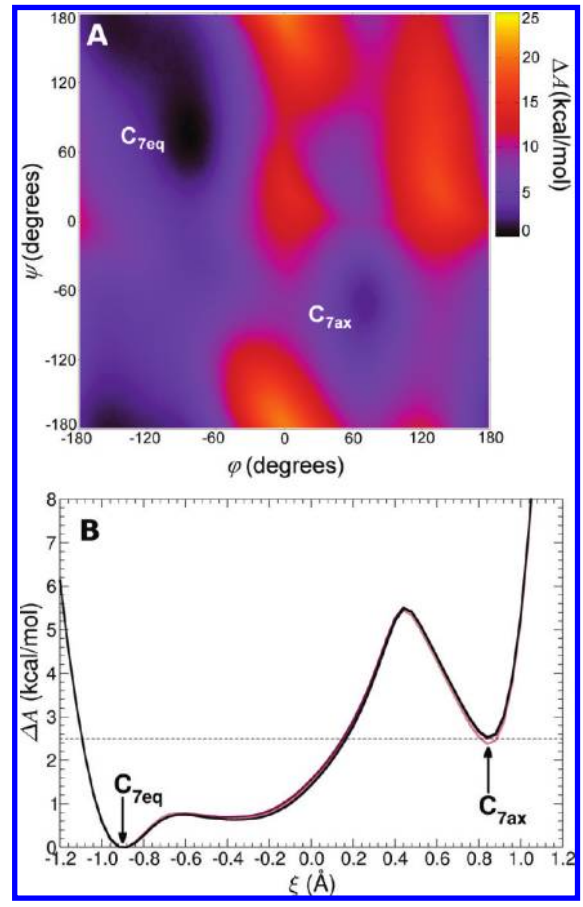


***Figure 1.*** (A) Two-dimensional ($\phi$, $\psi$) free energy landscape of *N*-acetyl-*N*′-methylalanylamide in the gas phase derived from a reference ABF calculation. (B) Free energy change along collective variable $\xi$ = rmsd($C_{7eq}$) − rmsd($C_{7ax}$), the difference between the distance rmsd with respect to the $C_{7eq}$ and $C_{7ax}$ conformational states. The free energy profiles are obtained from independent 20 (light curve), 20 (dark curve), and 40 ns (black curve) ABF simulations.

In the present work, determination of the two-dimensional free energy landscape of NANMA only represents the necessary preamble to an independent series of computations based on variables of higher collectivity than the mere $\phi$ and $\psi$ torsional angles of the backbone. However predictable, the results of these preliminary free energy calculations depicted in Figure 1 agree quantitatively with previous investigations; see, for instance, ref 96. In particular, ($\phi$, $\psi$)-integration over the basins corresponding to the $C_{7eq}$ and $C_{7ax}$ conformations, characterized by a long-lived intramolecular hydrogen bond, yields a free energy difference of 2.5 kcal/mol, in favor of the equatorial motif.[78,96]

The metadynamics calculation yields a free energy landscape identical to that determined by means of ABF (data not shown). Fast-relaxing, low-friction systems such as NANMA do not place high demands on the algorithms used to sample them, as demonstrated by early successes obtained

with limited sampling and unsophisticated algorithms. Metadynamics can be run with settings that result in high energy input (frequent accumulation of high hill potentials), without adverse consequences on the accuracy on the PMF. As a result, complete sampling can be obtained from a relatively short, 30 ns trajectory. As the ABF approach imposes that the system remains close to equilibrium, it requires a longer sampling time (100 ns). It is important to note, however, that this situation may not always occur in more delicate cases.

Transition between the lowest free energy states, $C_{7eq}$ and $C_{7ax}$, of NANMA has been the object of a number of computational investigations published in the past decade.[83–85,89] In a nutshell, three possible, low free energy pathways can be considered to describe the ($\phi$, $\psi$)-isomerization of the peptide. The first path connects the two conformations through the lowest point of the quasi-continuous free energy barrier arising around $\phi = 0°$. The second path uses the $C_5$, extended state as an intermediate between the $C_{7eq}$ and $C_{7ax}$ conformers, overcoming the free energy barrier located ca. $\phi = 120°$. Last, the third path partially overlaps with the previous one, yet, in lieu of diffusing in the wide basin that encompasses the $C_5$, $C_{7eq}$, and $\beta$ conformations, visits the higher free energy states of the right-handed α-helix region.

As can be observed in Figure 1, the three independent free energy calculations that rely upon the use of variable $\xi$ = rmsd($C_{7eq}$) − rmsd($C_{7ax}$) yield a consistent picture for the transition between $C_{7eq}$ and $C_{7ax}$. Although a longer, 40 ns simulation has been performed for reference purposes, 20 ns appears to be ample to achieve convergence of the free energy. Each free energy profile possesses two distinct minima positioned almost equidistantly with respect to $\xi$ = 0 Å and approximately 2.5 kcal/mol apart, in line with the measure based on the two-dimensional ($\phi$, $\psi$) map. Interestingly enough, the three different curves exhibit a shallow free energy minimum emerging around −0.4 Å, which corresponds to an ensemble of $C_5$-like, extended states. This pseudominimum prefaces an abrupt, 5.6 kcal/mol barrier toward the $C_{7ax}$ conformation, thereby suggesting that isomerization of NANMA proceeds through the second low free energy path outlined previously.

**Chloride Ion Permeation across a Peptide Nanotube.** Synthetic nanotubes resulting from the self-assembly of cyclic peptides are capable of conducting ions.[97] Synthesized with the proper amino-acid sequence, these nanotubes exhibit a pronounced tendency to insert as independent entities into the lipid bilayer, where they act as transmembrane channels.[98,99] Atomic-level mechanism and energetics of ion transport have been explored by means of complementary theoretical approaches.[100–102] In the light of calculations relying upon Poisson−Nernst−Planck theory, it has been suggested that conduction through open-ended tubular structures can be strongly modulated by the nature of the surroundings.[101,103,104] Such environmental effects on ion transport were subsequently quantified, employing free energy calculations, wherein a sodium ion was shuttled across the cavity of a peptide nanotube spanning the width of a fully hydrated POPC lipid bilayer.[26]

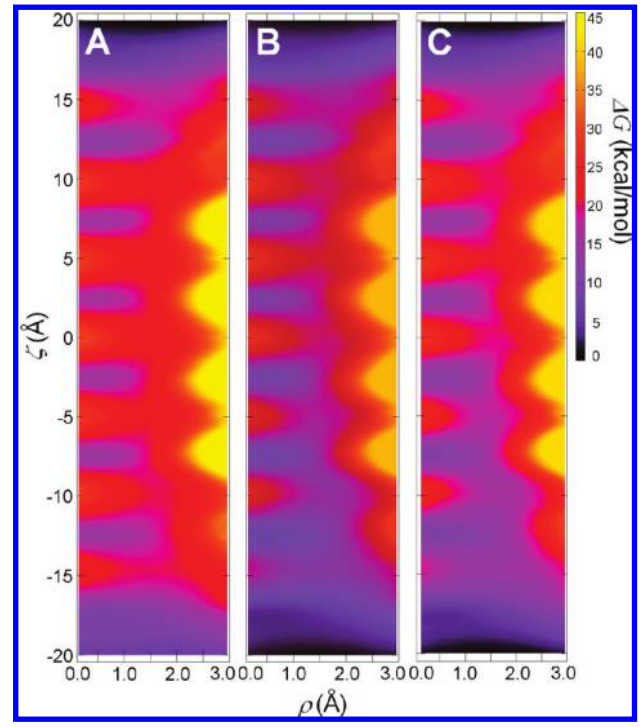


***Figure 2.*** Comparison of the two-dimensional free energy landscapes characterizing the transport of a chloride ion in a peptide nanotube spanning a fully hydrated POPC lipid bilayer, using ABF, without (A) and with (B) periodicity-enforced integration of the gradients, and metadynamics (C). The free energy is measured concomitantly along the radial, $\rho$, and the longitudinal, $\zeta$, directions of the membrane-spanning tubular structure.

In Figure 2, the two-dimensional ($\rho$, $\zeta$) free energy maps delineating the translocation of a chloride ion in the same tubular structure are displayed, based on separate ABF and metadynamics calculations. From a methodological standpoint, the striking resemblance between the measured free energy landscapes ought to be underlined. Periodicity-enforced integration of the gradients obtained from the ABF calculation yields a free energy map that is by and large fully superimposable on that generated with metadynamics. A glance at the ABF maps reconstructed with and without periodicity suggests that introduction of the latter when integrating the gradients somewhat reshapes the free energy landscape, altering its expected symmetry with respect to $\zeta$ = 0 Å.

In sharp contrast with sodium,[26] transport of chloride in the present peptide nanotube is markedly unfavorable. Translocation of the halide ion is burdened by a steep free energy barrier, on the order of 17 kcal/mol, at the mouth of the synthetic channel. This result is not completely surprising, given the radius of the pore formed by the stacked *cyclo*[LW]$_4$ peptide units, and the optimal aqueous coordination of chloride, found to be equal to ca. 6−8 at the experimental level,[105] and to about 7.5 on the basis of MD simulations in bulk water.[100] The significant free energy penalty arising at $\zeta = \pm 15$ Å is, therefore, linked to a severe dehydration of the halide ion, entering the synthetic channel partially "naked".

Diffusion of the ion is further hampered by subsequent free energy barriers, ca. 7−8 kcal/mol high, emerging at the

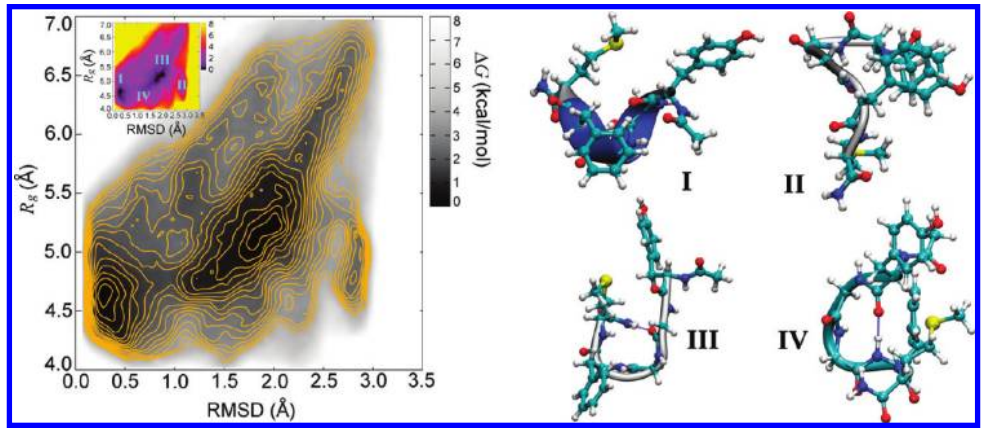


***Figure 3.*** Two-dimensional (rmsd, $R_g$) free energy landscape of Met-enkephalin in aqueous solution. The position rmsd with respect to a helical conformation is measured over α-carbon atoms only. The radius of gyration, $R_g$, is evaluated over all heavy, but α-carbon atoms. Contours of the main two-dimensional map are separated by 0.5 kcal/mol. The **I**−**IV** key conformations of Met-enkephalin are charted on the inset free energy landscape and depicted to the right as cartoon and ball-and-stick representations. In the cartoon representation, color indicates secondary structure. Molecular graphics were rendered with VMD.[109]

midpoint between two adjacent cyclic peptides, the separation of which amounts to about 4.7 Å. Congruent with the simulations of the sodium ion,[26] in-plane coordination appears to be also the energetically preferred state for chloride. It is remarkable that the halide ion does not hop between cyclic peptides following a rectilinear path, collinear to the long axis of the synthetic channel at $\zeta = 0$ Å, but instead grazes the wall of the latter to form intermittent interactions with peptide amino moieties. This diffusion mode is reflected in a curvilinear low-free energy path apparent in Figure 2.

**Structure of Met-enkephalin in an Aqueous Solution.** On account of its unusual flexibility, Met-enkephalin can bind interchangeably either the $\delta$, the $\kappa$, or the $\mu$-opioid receptor, where it is anticipated to adopt distinct conformations. This, in large measure, rationalizes why experimental approaches have hitherto failed to propose a converging view of the native structure of this short peptide.[26,106,107] Although it is reasonable to believe that the marked flexibility of the backbone would be reflected in a generally flat free energy landscape, equilibrium MD simulations at a single temperature have proven to prevent exhaustive exploration of conformational space, the peptide chain being recurrently trapped kinetically in a random, unrepresentative conformation.[60] Despite its reduced length, Met-enkephalin, therefore, constitutes a pathological case for standard MD, but a well-suited candidate for more recent, multicanonical approaches, like replica-exchange MD,[108] aimed at enhancing ergodic sampling.

The two-dimensional free energy map of Figure 3 sheds light on the conformational space accessible to the short peptide along the directions of the position rmsd with respect to an arbitrary chosen helical motif and of the radius of gyration of the backbone. As has been commented on previously,[67] the free energy landscape of Met-enkephalin in aqueous solution consists of a rather wide, shallow basin, featuring a number of pronounced minima. At low distance rmsd and $R_g$, a compact, $3_{10}$-helix motif (**I**) is observed, resulting primarily from the formation of an intramolecular hydrogen bond between the carbonyl group of residue $i$ and the amino group of residue $i + 3$, albeit transitory interconversion to an α-helical $i$ to $i + 4$ hydrogen bond can be detected. Still at low $R_g$, but at a larger distance rmsd, around 2.8 Å, a free energy minimum (**II**) corresponding to an embryonic helix turn emerges about 2.1 kcal/mol higher than that of conformation **I**. A third minimum (**III**) can be found at a distance rmsd of 2.0 Å and an $R_g$ of 5.2 Å, with a free energy equal to that of the helical motif **I** within statistical accuracy. Its U-shaped structure is essentially nonhelical, featuring an intermittent hydrogen bond formed between the terminal, blocking amino moiety and the carbonyl group of the first glycine residue. Last, a fourth conformational minimum (**IV**) can be found at a distance rmsd of 1.4 Å and an $R_g$ of 4.8 Å, and corresponds to a free energy only 0.6 kcal/mol above that of structures **I** and **III**. In this free energy minimum, the peptide chain adopts a $\gamma$-turn conformation, often encountered in $\beta$-hairpin motifs.

It is apparent from the present results that, using a reduced set of collective variables and a single temperature, ABF is able to recover the complete free energy landscape of Met-enkephalin, virtually identical to that reported by Sanbonmatsu and Garcia on the basis of parallel-tempering MD simulations.[67] The (rmsd, $R_g$) two-dimensional map confirms, indeed, that this free energy landscape is relatively shallow and consists of essentially four distinct ensembles of conformations characterized by overall comparable free energies, barring structure **II**, and separated by appreciably low barriers.

The local minima are primarily distinguished by their rmsd value. Therefore, in this case, the second collective variable, $R_g$, is not essential to resolve the low free energy states, but it accelerates the sampling of transition pathways between them, and therefore the overall convergence of the calculation. The rmsd could be considered a one-dimensional reaction coordinate, while $R_g$ is a degree of freedom in the orthogonal space that is included in the ABF calculation for numerical efficiency.

**Conformational Free Energy Landscape of Deca-alanine.** Deca-alanine in vacuum has been used several times as a computationally inexpensive and seemingly simple toy

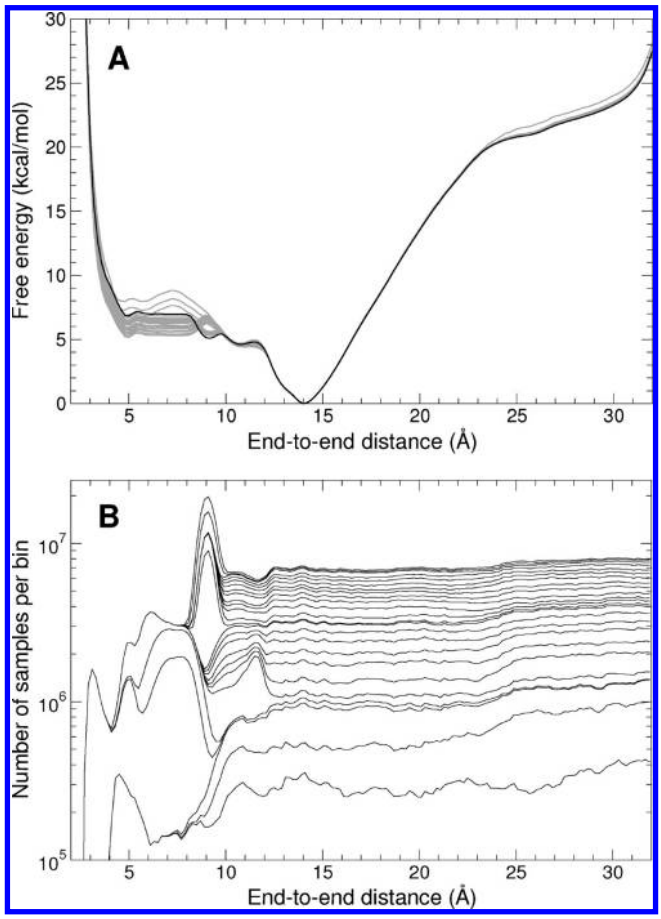


***Figure 4.*** (A) One-dimensional free energy profile of deca-alanine in vacuum, as a function of the end-to-end distance. Intermediate results are plotted for every 20 ns period as gray lines; the final result of the 500 ns ABF simulation is shown as a dark line. (B) Sampling histograms (on a logarithmic scale) corresponding to the one-dimensional ABF simulation of deca-alanine. Each line is the full histogram at the end of a 20 ns period of the simulation.

model for conformational free energy calculations on peptides.[6,28,110–113] Stretching the peptide from its native, α-helical state to extended conformations, and back, is indeed a fairly straightforward transformation, for which relatively few pathways are possible. All simulations cited above, using the end-to-end distance of the peptide chain as a coordinate and various biasing schemes, achieve convergence and find potentials of mean force in good agreement with one another. Such simulations, however, only explore a small fraction of the conformational space available to deca-alanine. Indeed, when an attempt was made to sample the more compact conformations corresponding to end-to-end distances shorter than the α-helix length (i.e., less than 12 Å), it was found that several local minima, and the complex pathways linking them, were not resolved by that simple distance parameter. As a result, the complete free energy landscape of the peptide could not be mapped.[28]

As can be seen from Figure 4B, using ABF to sample the end-to-end coordinate $d$ provides very uniform histograms for elongated structures, and uneven, sporadic sampling of the compact region. Thus, the potential of mean force shown in Figure 4A, while very accurate for $d$ greater than 12 Å, is not converged for smaller values. Furthermore, it does not exhibit clear features that could be related to the metastable conformations that can be identified in that region. The reason behind such nonuniform sampling of the low-$d$ range is that $d$ is a highly degenerate descriptor of most of the conformational space of deca-alanine. Even with an ideally converged adaptive bias canceling the free energy profile, some of the transitions would remain rare events, essentially because the enthalpic or entropic barriers are orthogonal to the direction of the bias.

Unbiased simulations starting from structures chosen from the ABF simulations indicate several metastable conformers whose lifetime is at least 30 ns. In order of increasing relative potential energy, these structures are the α-helix (0 kcal/mol), a loop containing a short $3_{10}$-helical segment (3.5 kcal/mol), an $\omega$-shaped loop composed of $\beta$ and other turns (6.2 kcal/mol), a $\beta$-bridged loop (9.3 kcal/mol), a $\beta$-hairpin (9.8 kcal/mol), and a slightly expanded $\pi$-helix featuring transient $i$ to $i + 5$ hydrogen bonds (11 kcal/mol). These conformations are represented in Figure 6.

To resolve the compact states that are merged in the one-dimensional landscape, the distance parameter was supplemented with a second degree of freedom, the position rmsd from a typical $\beta$-hairpin conformation. The results are represented in Figure 5. Although a large fraction of the reduced space is visited, sampling tends to accumulate in a few localized regions (Figure 5B), suggesting a failure of the collective variables to describe all of the free energy barriers in these regions. The global free energy minimum corresponding to the α-helix is clearly visible in the measured free energy landscape (Figure 5A). In contrast, the basins corresponding to metastable structures are almost coalesced and separated by low barriers, inconsistent with the long lifetimes of these conformers. Despite its limits, the two-dimensional profile is consistent with the one-dimensional free energy of 4 in the region containing the α-helix and the extended states.

Finally, a set of three RMSDs was chosen to try and resolve the numerous conformers of similar compactness of deca-alanine. The three-dimensional PMF is shown in Figure 6. In general, the differences in free energy between the metastable conformers and the α-helix are smaller than the potential energy differences, indicating significant entropy−enthalpy compensation. Indeed, the α-helix is more rigid than the other conformers. Because of the width of basins corresponding to individual conformers, and the short distance separating them in the reduced space, some conformers are still not perfectly resolved, in particular in the low free energy region containing the $\beta$-hairpin and $\beta$-bridge structures. Indeed, the local free energy minimum in that region contains conformations similar to both structures, whose similarity renders difficult to distinguish in a low-dimension representation. The free energy landscape is, however, sufficiently resolved for the complete conformational space to be explored at a much increased rate due to the adaptive bias. Here, because the full conformation space of flexible peptide is explored, the rmsd coordinate is not robust over its entire range. Specifically, at very high rmsd values, the structure becomes too dissimilar from the

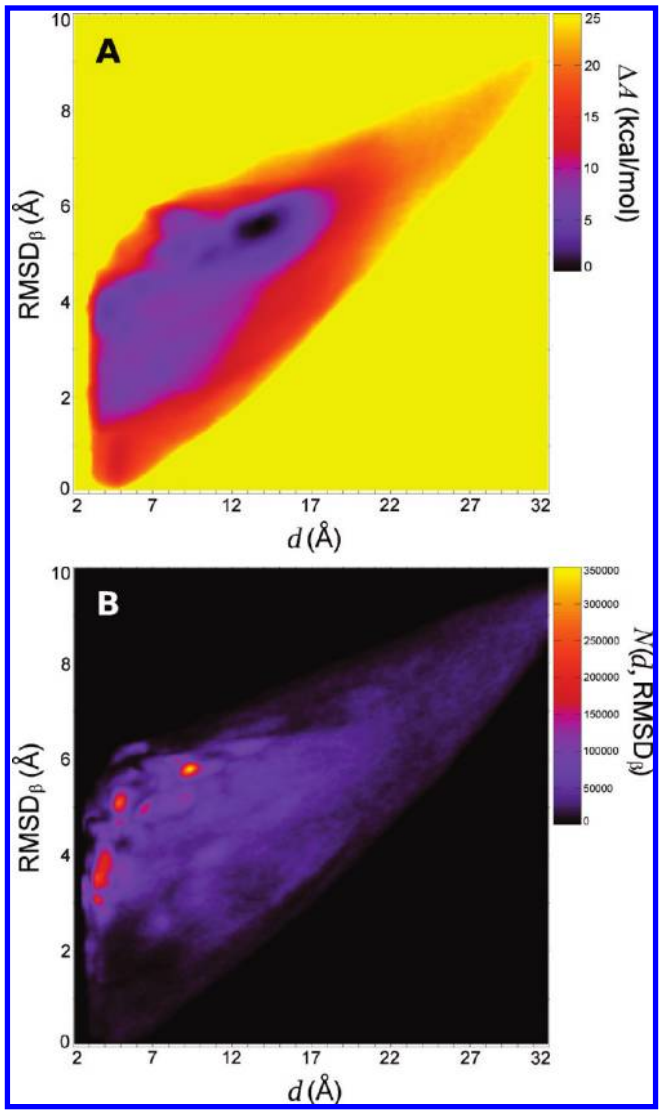


***Figure 5.*** Two-dimensional ABF description of the conformations of deca-alanine in vacuum. The variables used for ABF are the end-to-end distance and the position rmsd with respect to a $\beta$-hairpin conformation. (A) Free energy landscape. (B) Sampling histogram at the end of the 200 ns simulation.

reference coordinates for the optimal rotation to be uniquely defined. In such regions of conformation space, the gradient of the rmsd is irregular and exhibits jumps, and hence forces measured or applied along that direction have little physical significance. It should nevertheless be noted that in more realistic applications, the relevant range of the rmsd will typically be limited to the region where the optimal rotation is unique, hence avoiding the issue altogether.

Deca-alanine exhibits a very structured, corrugated free energy landscape, featuring a rich set of metastable conformers. Although the peptide is of little intrinsic biochemical relevance, particularly in vacuum, it proves to be a challenging test case for conformational sampling algorithms.

**Comparison of ABF and Metadynamics.** The ABF and metadynamics schemes rely on several comparable parameters. The choice of collective variables is crucial in both cases. Metadynamics offers more flexibility in the choice and implementation of collective variables, because only the value and gradient of the variables are needed, not their second derivatives. In the present implementation, any set of variables can be used together: there is no orthogonality requirement. Both methods require a width parameter, the Gaussian hill width in metadynamics and the bin width in ABF. This parameter defines the spatial resolution of both the time-dependent bias and the final PMF. Finally, a metadynamics simulation can be characterized by a filling rate, equal to the height of the Gaussian potential increments divided by the period of addition of such increments. This parameter controls how much work is performed on the system by the bias, and this quantity is typically constant for the complete duration of the simulation. The corresponding parameter of ABF, the threshold amount of sampling before the adaptive bias is enabled, is not equivalent to the filling rate. It has the dimension of a time rather than that of a power, and it only affects the initial behavior of the simulation. Once the amount of sampling is above that threshold, and neglecting the finite resolution of the lattice, the behavior of ABF is entirely specified by the algorithm, regardless of the values of tunable parameters.

In biased simulations that rely on reduced representations comprising few degrees of freedom, the most common shortcoming is the slow relaxation of other, "hidden" degrees of freedom, not included in the chosen set of collective variables. Under these premises, the underlying energy landscape of a given point in reduced space may change during the simulation, with the result that data collected previously become "stale", at least on the time scale of assisted diffusion in reduced space.[24] In principle, in the limit of ergodic sampling, even the slowest degrees of freedom are fully thermalized and convergence occurs. In practice, however, achieving this situation is highly dependent on the relevance of the reduced space as a reaction coordinate.

In any such nonideal situation, the exact form of history dependence of the biasing algorithm comes into play. Metadynamics is almost always performed with a constant height of the Gaussian hills, chosen to meet the desired accuracy through a theoretical estimate of the error.[114,115] This gives the method a finite memory time, which can be identified as the time required to explore the whole landscape. In this case, if relaxation of hidden degrees of freedom modifies the potential seen by the collective variables, metadynamics will fill up the minima of the "new" free energy landscape, until all memory of the previous landscape has been erased. It seems possible that such a situation might give rise to a cyclic behavior, where the locally measured free energy (on the time scale of metadynamics) oscillates between values corresponding to different basins, as dictated by transitions of hidden, slow degrees of freedom. This behavior might, however, be viewed as useful, in that it allows the method to recover from situations where inaccurate data have been collected, either as a result of deficiencies in the reduced representation or due to irreversible work performed by the metadynamics bias.

ABF, in contrast, has an effectively infinite memory time. Once a data point has been accumulated in the average, its weight decreases as the inverse of the total number of samples, that is, as $1/t$. For this reason, the oscillating behavior described above is unlikely. Instead, a commonly

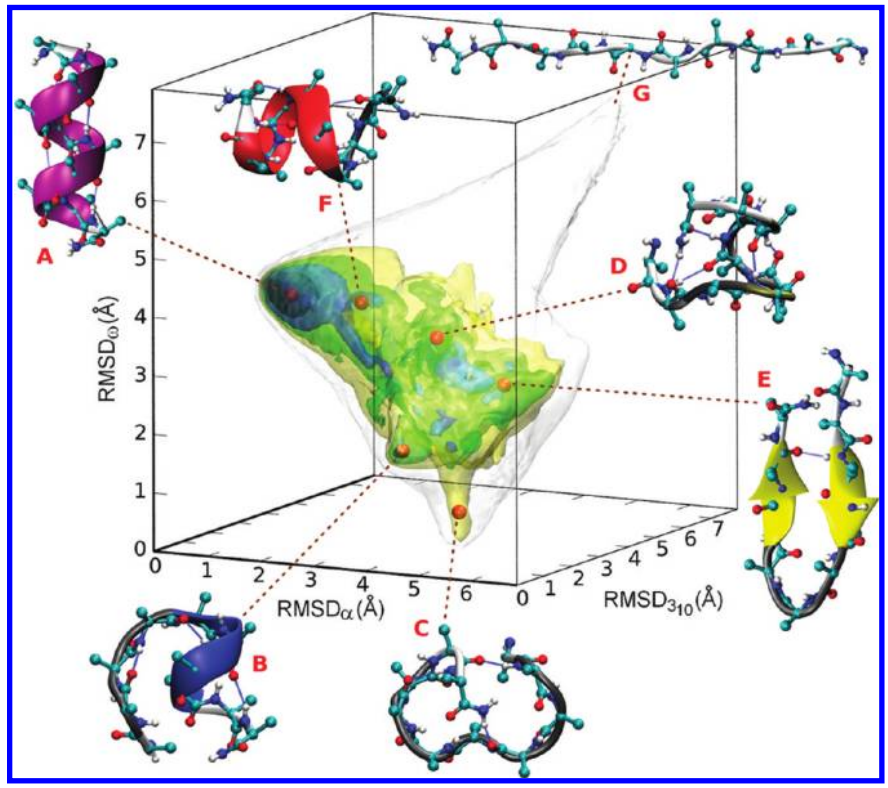


***Figure 6.*** Three-dimensional conformational free energy landscape of deca-alanine, as a function of the rmsd with respect to ideal α-helical, $\omega$-shaped $\gamma$-turn, and turn/$3_{10}$-helix conformations, respectively. The free energy was computed by numerically integrating the gradient obtained from a 400 ns ABF simulation. Free energy isosurfaces are shown for respective values of 3 (black), 6 (blue), 9 (green), 12 (yellow), and 24 kcal/mol (white). Average positions corresponding to metastable conformations are indicated by red spheres. Conformers are shown as ball-and-stick and cartoon representations, with color indicating secondary structure (purple, α-helix; blue, $3_{10}$-helix; red, $\pi$-helix; gray, turn; yellow, $\beta$-strand; tan, $\beta$-bridge; white, unstructured). Hydrogen bonds are indicated as blue lines. The conformers are labeled using red capital letters: (A) α-helix, (B) turn/$3_{10}$-helix, (C) $\omega$-shaped turn, (D) $\beta$-bridge, (E) $\beta$-hairpin, (F) $\pi$-helix, and (G) extended form (unstable).

observed effect of slowly relaxing hidden degrees of freedom is a change of the sampling behavior as the simulation progresses. Over time, the relative weight of newly accrued data in the average decreases, as does the responsiveness of the time-dependent bias to changes in the locally measured thermodynamic force. This is the desired behavior in the ideal context of a perfect reaction coordinate space, where all orthogonal degrees of freedom are either fast, or kinetically trapped and not relevant to the transformation under study. In real cases, the symptom is an initially efficient exploration of reduced space, followed by an increasing tendency to get trapped in local minima as they are "discovered" through relaxation in the orthogonal space and crossing of hidden barriers. This is observed, to a minor extent, in the 2D and 3D deca-alanine simulations described in the previous sections. Arguably, such behavior is indicative of failure of the reduced space to capture the reactive intermediates and pathways to a degree that allows for sampling over the intended (or technically feasible) time scale.

Metadynamics is designed as a nonequilibrium method, whereas ABF relies on equilibrium sampling from the canonical ensemble. In practice, ABF simulations go through an initial stage during which the estimate of the local free energy gradient evolves rapidly; then the running average is updated on a much slower scale, and eventually stabilizes altogether. Applying a biasing force based on the early, fast-fluctuating estimate of the free energy gradient may push the dynamics into a nonequilibrium regime. This initial departure from equilibrium conditions can be greatly reduced in practice by delaying the introduction of the biasing force until after the large fluctuations of the running average have ended: this is accomplished by waiting for a preset number of samples to be accrued in a local bin.[6,8,28] Should any nonequilibrium effects occur, however, force samples measured in that phase are still taken into account in the average, and, as mentioned above, this contribution never vanishes. Any bias (typically, an overestimated free energy gradient) due to irreversible work performed in the beginning of the simulation will taint the final data, with a weight that only decays as $1/t$. In contrast, exponential convergence of ABF has only been proved under somewhat restrictive assumptions, including the use of a large number of replicas.[116] When a metadynamics run is carried out with constant hill height, irreversible work is performed throughout the simulation. This contribution may only be deemed to have been eliminated from the measured PMF once multiple sweeps have been observed (or, in higher dimension, multiple transitions between neighboring basins).

Both issues (slow hidden variables and irreversible work) can be alleviated by restricting the data set used to reconstruct the free energy, eliminating selected, problematic data. In metadynamics, this is achieved by stopping the simulation once the system leaves the relevant region of configuration space. In ABF, data collected in the initial, out-of-equilibrium

stage can be removed from the final average. Metadynamics performs well in low-friction systems such as the peptide nanotube example, because the filling rate (hill height divided by the hill accumulation period) can be increased while maintaining a level of irreversible work that does not hinder convergence.

## Conclusion

An implementation of the ABF approach supporting multidimensional reaction coordinates based on sophisticated variables is proposed. This implementation is available in the scalable molecular-dynamics program NAMD, but can be readily incorporated into any MD platform. The method and its implementation have been tested on a variety of biomolecular systems. Multidimensional reaction descriptors improve the level of detail in which molecular processes can be mapped, as in the case of chloride permeation through a self-assembled peptide nanotube. In systems featuring particularly complex free energy landscapes, such as the multiple metastable conformations of deca-alanine, efficient sampling is only possible when applying the adaptive bias in a two- or three-dimensional reduced space. The work of constructing an appropriate reduced representation is made easier by the availability of variables such as the position rmsd, and the flexibility afforded by linear combinations of predefined variables.

Two of the test cases were used to compare directly ABF and the metadynamics method, applied on the same variables, under otherwise identical simulation conditions. Both approaches yield the expected results in terms of phase space exploration and sampling, and reconstruction of the free energy landscape. Neither can be said to be more efficient or accurate than the other on general grounds. Still, metadynamics does offer an inexpensive way to rapidly explore simple, fast-relaxing systems that are robust enough to withstand a high energy input, as is apparent from the toy model of NANMA, while ABF may constitute a safer option for more fragile systems. Differences are likely to become most apparent in difficult scenarios, where the two approaches react differently to incomplete sampling and nonequilibrium effects. Whereas metadynamics is much more likely to perform significant irreversible work in late stages of such simulations, ABF may become inefficient and sample reduced regions for disproportionate times.

The most crucial issue remains the choice of a reaction coordinate space. As illustrated in the deca-alanine example, describing a small system with seemingly limited phase space may require multiple parameters, fine-tuned to resolve nearby points of conformation space that, nevertheless, belong to different low free energy basins or pathways. More sophisticated collective variables will be developed to describe complex, frustrated free energy landscapes. The existing algorithms will evolve toward better scalability, or be replaced altogether by new sampling methods. In any event, it is essential for the progress of large-scale applications that new developments in sampling and free energy algorithms be kept in phase with state-of-the-art, parallel simulation software.

**Acknowledgment.** J.H., G.F., and M.L.K. acknowledge funding from the National Institutes of Health. We are grateful to Dr. Tony Lelièvre for enlightening discussions, and to Drs. Christopher Harrison and Peter Freddolino for their help with the implementation and testing of numerical methods.

### References

(1) Rodinger, T.; Pomès, R. *Curr. Opin. Struct. Biol.* **2005**, *15*, 164–170.

(2) *Free Energy Calculations. Theory and Applications in Chemistry and Biology*; Chipot, C., Pohorille, A., Eds.; Springer Verlag: New York, 2006.

(3) Lei, H.; Duan, Y. *Curr. Opin. Struct. Biol.* **2007**, *17*, 187–191.

(4) Laio, A.; Parrinello, M. *Proc. Natl. Acad. Sci. U.S.A.* **2002**, *99*, 12562–12565.

(5) Bonomi, M.; Branduardi, D.; Bussi, G.; Camilloni, C.; Provasi, D.; Raiteri, P.; Donadio, D.; Marinelli, F.; Pietrucci, F.; Broglia, R. A.; Parrinello, M. PLUMED: a portable plugin for free-energy calculations with molecular dynamics; 2009; arXiv:0902.0874v3 [physics.comp-ph]; arXiv.org ePrint archive, http://www.arXiv.org/abs/0902.0874 (accessed Nov. 9, 2009).

(6) Hénin, J.; Chipot, C. *J. Chem. Phys.* **2004**, *121*, 2904–2914.

(7) Darve, E.; Pohorille, A. *J. Chem. Phys.* **2001**, *115*, 9169–9183.

(8) Darve, E.; Rodríguez-Gómez, D.; Pohorille, A. *J. Chem. Phys.* **2008**, *128*, 144120.

(9) Phillips, J. C.; Braun, R.; Wang, W.; Gumbart, J.; Tajkhorshid, E.; Villa, E.; Chipot, C.; Skeel, R. D.; Kalé, L.; Schulten, K. *J. Comput. Chem.* **2005**, *26*, 1781–1802.

(10) Hénin, J.; Pohorille, A.; Chipot, C. *J. Am. Chem. Soc.* **2005**, *127*, 8478–8484.

(11) Xu, J.; Crowley, M. F.; Smith, J. C. *Protein Sci.* **2009**, *18*, 949–959.

(12) Halling-Brown, M. D.; Moss, D. S.; Sansom, C. E.; Shepherd, A. J. *Philos. Trans. R. Soc. London, Ser. A* **2009**, *367*, 2705–2716.

(13) Weronski, P.; Jiang, Y.; Rasmussen, S. *Biophys. J.* **2007**, *92*, 3081–3091.

(14) Gorfe, A. A.; Babakhani, A.; McCammon, J. A. *Angew. Chem., Int. Ed.* **2007**, *46*, 8234–8237.

(15) Gorfe, A. A.; McCammon, J. A. *J. Am. Chem. Soc.* **2008**, *130*, 12624–12625.

(16) Vaitheeswaran, S.; Thirumalai, D. *Proc. Natl. Acad. Sci. U.S.A.* **2008**, *105*, 17636–17641.

(17) Yu, Y.; Chipot, C.; Cai, W.; Shao, X. *J. Phys. Chem. B* **2006**, *110*, 6372–6378.

(18) Cai, W.; Sun, T.; Liu, P.; Chipot, C.; Shao, X. *J. Phys. Chem. B* **2009**, *113*, 7836–7843.

(19) Rodriguez, J.; Elola, M. D. *J. Phys. Chem. B* **2009**, *113*, 1423–1428.

(20) Rodriguez, J.; Semino, R.; Laria, D. *J. Phys. Chem. B* **2009**, *113*, 1241–1244.

(21) Treptow, W.; Tarek, M. *Biophys. J.* **2006**, *90*, L64–L66.

(22) Lamoureux, G.; Klein, M. L.; Berneche, S. *Biophys. J.* **2007**, *92*, L82–L84.

(23) Ivanov, I.; Cheng, X.; Sine, S. M.; McCammon, J. A. *J. Am. Chem. Soc.* **2007**, *129*, 8217–8224.

(24) Hénin, J.; Tajkhorshid, E.; Schulten, K.; Chipot, C. *Biophys. J.* **2008**, *94*, 832–839.

(25) Dehez, F.; Pebay-Peyroula, E.; Chipot, C. *J. Am. Chem. Soc.* **2008**, *130*, 12725–12733.

(26) Dehez, F.; Tarek, M.; Chipot, C. *J. Phys. Chem. B* **2007**, *111*, 10633–10635.

(27) Hénin, J.; Shinoda, W.; Klein, M. *J. Phys. Chem. B* **2008**, *112*, 7008–7015.

(28) Chipot, C.; Hénin, J. *J. Chem. Phys.* **2005**, *123*, 244906.

(29) Hénin, J.; Schulten, K.; Chipot, C. *J. Phys. Chem. B* **2006**, *110*, 16718–16723.

(30) Lee, E. H.; Hsin, J.; Mayans, O.; Schulten, K. *Biophys. J.* **2007**, *93*, 1719–1735.

(31) Blumberger, J.; Lamoureux, G.; Klein, M. L. *J. Chem. Theory Comput.* **2007**, *3*, 1837–1850.

(32) Kuang, Z.; Mahankali, U.; Beck, T. L. *Proteins* **2007**, *68*, 26–33.

(33) Spiegel, K.; Magistrato, A.; Carloni, P.; Reedijk, J.; Klein, M. L. *J. Phys. Chem. B* **2007**, *111*, 11873–11876.

(34) Zheng, L.; Chen, M.; Yang, W. *Proc. Natl. Acad. Sci. U.S.A.* **2008**, *105*, 20227–20232.

(35) Zheng, L.; Chen, M.; Yang, W. *J. Chem. Phys.* **2009**, *130*, 234105.

(36) *IUPAC Compendium of Chemical Terminology*, 2nd ed. (the "Gold Book"); McNaught, A. D., Wilkinson, A., Eds.; Blackwell Scientific Publications: Oxford, 1997.

(37) Kirkwood, J. G. *J. Chem. Phys.* **1935**, *3*, 300–313.

(38) Zwanzig, R. W. *J. Chem. Phys.* **1954**, *22*, 1420–1426.

(39) Ciccotti, G.; Ferrario, M.; Hynes, J. T.; Kapral, R. *Chem. Phys.* **1989**, *129*, 241–251.

(40) Carter, E, A.; Ciccotti, G.; Hynes, J. T.; Kapral, R. *Chem. Phys. Lett.* **1989**, *156*, 472–477.

(41) Ruiz-Montero, M. J.; Frenkel, D.; Brey, J. J. *Mol. Phys.* **1997**, *90*, 925–941.

(42) den Otter, W. K.; Briels, W. J. *J. Chem. Phys.* **1998**, *109*, 4139–4146.

(43) den Otter, W. K. *J. Chem. Phys.* **2000**, *112*, 7283–7292.

(44) Ciccotti, G.; Kapral, R.; Vanden-Eijnden, E. *ChemPhysChem* **2005**, *6*, 1809–1814.

(45) Maragliano, L.; Vanden-Eijnden, E. *J. Chem. Phys.* **2008**, *128*, 184110.

(46) Grubmüller, H. *Phys. Rev. E* **1995**, *52*, 2893–2906.

(47) Bhandarkar, M.; Brunner, R.; Buelens, F.; Chipot, C.; Dalke, A.; Dixit, S.; Fiorin, G.; Freddolino, P.; Grayson, P.; Gullingsrud, J.; Gursoy, A.; Hardy, D.; Harrison, C.; Hénin, J.; Humphrey, W.; Hurwitz, D.; Krawetz, N.; Kumar, S.; Nelson, M.; Phillips, J.; Shinozaki, A.; Zheng, G.; Zhu, F. *NAMD user's guide, version 2.7*; Theoretical biophysics group, University of Illinois and Beckman Institute: Urbana, IL, 2009.

(48) Feller, S. E.; Zhang, Y. H.; Pastor, R. W.; Brooks, B. R. *J. Chem. Phys.* **1995**, *103*, 4613–4621.

(49) Darden, T. A.; York, D. M.; Pedersen, L. G. *J. Chem. Phys.* **1993**, *98*, 10089–10092.

(50) Tuckerman, M. E.; Berne, B. J.; Martyna, G. J. *J. Phys. Chem. B* **1992**, *97*, 1990–2001.

(51) MacKerell, A. D., Jr. *J. Phys. Chem. B* **1998**, *102*, 3586–3616.

(52) Jorgensen, W. L.; Chandrasekhar, J.; Madura, J. D.; Impey, R. W.; Klein, M. L. *J. Chem. Phys.* **1983**, *79*, 926–935.

(53) Rossky, P. J.; Karplus, M. *J. Am. Chem. Soc.* **1979**, *101*, 1913.

(54) Ramachandran, G.; Ramakrishnan, C.; Sasisekharan, V. *J. Mol. Biol.* **1963**, *7*, 95–99.

(55) Ghadiri, M. R.; Granja, J. R.; Buehler, L. K. *Nature* **1994**, *369*, 301–304.

(56) Hartgerink, J. D.; Granja, J. R.; Milligan, R. A.; Ghadiri, M. R. *J. Am. Chem. Soc.* **1996**, *118*, 43–50.

(57) Bong, D. T.; Clark, T. D.; Granja, J. R.; Ghadiri, M. R. *Angew. Chem., Int. Ed.* **2001**, *40*, 988–1011.

(58) Roques, B. P.; Garbay-Jaureguiberry, C.; Bajusz, S.; Maigret, B. *Eur. J. Biochem.* **1980**, *113*, 105–119.

(59) Li, Z.; Scheraga, H. A. *Proc. Natl. Acad. Sci. U.S.A.* **1987**, *84*, 6611–6615.

(60) Perez, J. J.; Villar, H. O.; Loew, G. H. *J. Comput.-Aided Mol. Des.* **1992**, *6*, 175–190.

(61) Koča, J.; Carlsen, P. H. J. *J. Mol. Struct. (THEOCHEM)* **1995**, *337*, 17–24.

(62) Bartels, C.; Karplus, M. *J. Phys. Chem. B* **1998**, *102*, 865–880.

(63) Carlacci, L. *J. Comput.-Aided Mol. Des.* **1998**, *12*, 195–213.

(64) Mitsutake, A.; Hansmann, U. H.; Okamoto, Y. *J. Mol. Graphics Modell.* **1998**, *16*, 226–38, 262−3.

(65) Hansmann, U. H.; Okamoto, Y.; Onuchic, J. N. *Proteins* **1999**, *34*, 472–483.

(66) Shen, M.-y.; Freed, K. F. *Biophys. J.* **2002**, *82*, 1791–1808.

(67) Sanbonmatsu, K. Y.; García, A. E. *Proteins: Struct., Funct., Genet.* **2002**, *46*, 225–234.

(68) Evans, D. A.; Wales, D. J. *J. Chem. Phys.* **2003**, *119*, 9947–9955.

(69) Zaman, M. H.; Shen, M. Y.; Berry, R. S.; Freed, K. F. *J. Phys. Chem. B* **2003**, *107*, 1685–1691.

(70) Berg, B. A.; Hsu, H.-P. *Phys. Rev. E* **2004**, *69*, 026703.

(71) Zhan, L. X.; Chen, J. Z. Y.; Liu, W. K. *Biophys. J.* **2006**, *91*, 2399–2404.

(72) Ramya, L.; Gautham, N. *J. Chem. Theory Comput.* **2009**, *5*, 2180–2190.

(73) Hagler, A. T.; Honig, B. *Proc. Natl. Acad. Sci. U.S.A.* **1978**, *75*, 554.

(74) Brady, J.; Karplus, M. *J. Am. Chem. Soc.* **1985**, *107*, 6103.

(75) Mezei, M.; Mehrotra, P. K.; Beveridge, D. L. *J. Am. Chem. Soc.* **1985**, *107*, 2239.

(76) Ravishanker, G.; Mezei, M.; Beveridge, D. L. *J. Comput. Chem.* **1986**, *7*, 345.

(77) Anderson, A.; Hermans, J. *Proteins: Struct., Funct., Genet.* **1988**, *3*, 262.

(78) Tobias, D. J.; Brooks, C. L. *J. Phys. Chem.* **1992**, *96*, 3864–3870.

(79) Pellegrini, M.; Grønbech-Jensen, N.; Doniach, S. *J. Chem. Phys.* **1996**, *104*, 8639.

(80) Neria, E.; Fischer, S.; Karplus, M. *J. Chem. Phys.* **1996**, *105*, 1902.

(81) Bartels, C.; Karplus, M. *J. Comput. Chem.* **1997**, *18*, 1450–1462.

(82) Chipot, C.; Pohorille, A. *J. Phys. Chem. B* **1998**, *102*, 281–290.

(83) Smith, P. E. *J. Chem. Phys.* **1999**, *111*, 5568–5579.

(84) Apostolakis, J.; Ferrara, P.; Caflisch, A. *J. Chem. Phys.* **1999**, *110*, 2099–2108.

(85) Bolhuis, P. G.; Dellago, C.; Chandler, D. *Proc. Natl. Acad. Sci. U.S.A.* **2000**, *97*, 5877–5882.

(86) Andricioaei, I.; Dinner, A. R.; Karplus, M. *J. Chem. Phys.* **2003**, *118*, 1074–1084.

(87) Chekmarev, D.; Ishida, T.; Levy, R. M. *J. Phys. Chem. B* **2004**, *108*, 19487–19495.

(88) Jang, H.; Woolf, T. B. *J. Comput. Chem.* **2006**, *27*, 1136–1141.

(89) Branduardi, D.; Gervasio, F. L.; Parrinello, M. *J. Chem. Phys.* **2007**, *126*, 054103.

(90) Neale, C.; Rodinger, T.; Pomes, R. *Chem. Phys. Lett.* **2008**, *460*, 375–381.

(91) Kwac, K.; Lee, K. K.; Han, J. B.; Oh, K. I.; Cho, M. *J. Chem. Phys.* **2008**, *128*, 105106.

(92) Feig, M. *J. Chem. Theory Comput.* **2008**, *4*, 1555–1564.

(93) Velez-Vega, C.; Borrero, E. E.; Escobedo, F. A. *J. Chem. Phys.* **2009**, *130*, 225101.

(94) Torrie, G. M.; Valleau, J. P. *J. Comput. Phys.* **1977**, *23*, 187–199.

(95) Kumar, S.; Bouzida, D.; Swendsen, R. H.; Kollman, P. A.; Rosenberg, J. M. *J. Comput. Chem.* **1992**, *13*, 1011–1021.

(96) Rosso, L.; Abrams, J. B.; Tuckerman, M. E. *J. Phys. Chem. B* **2005**, *109*, 4162–4167.

(97) Sánchez-Quesada, J.; Isler, M. P.; Ghadiri, M. R. *J. Am. Chem. Soc.* **2002**, *124*, 10004–10005.

(98) Kim, H. S.; Hartgerink, J. D.; Ghadiri, M. R. *J. Am. Chem. Soc.* **1998**, *120*, 4417–4424.

(99) Tarek, M.; Maigret, B.; Chipot, C. *Biophys. J.* **2003**, *85*, 2287–2298.

(100) Asthagiri, D.; Bashford, D. *Biophys. J.* **2002**, *82*, 1176–1189.

(101) Hwang, H.; Schatz, G. C.; Ratner, M. A. *J. Phys. Chem. B* **2006**, *110*, 6999–7008.

(102) Hwang, H.; Schatz, G. C.; Ratner, M. A. *J. Phys. Chem. B* **2006**, *110*, 26448–26460.

(103) Mamonov, A. B.; Coalson, R. D.; Nitzan, A.; Kurnikova, M. G. *Biophys. J.* **2003**, *84*, 3646–3661.

(104) Aguilella-Arzo, M.; Aguilella, V. M.; Eisenberg, R. S. *Eur. Biophys. J.* **2005**, *34*, 314–322.

(105) Marcus, Y. *Ion Solvation*; Wiley and Sons: London, 1985.

(106) Khaled, M. A.; Long, M. M.; Thompson, W. D.; Bradley, R. J.; Brown, G. B.; Urry, D. W. *Biochem. Biophys. Res. Commun.* **1976**, *76*, 224–231.

(107) Smith, G. D.; Griffin, J. F. *Science* **1978**, *199*, 1214–1216.

(108) Sugita, Y.; Okamoto, Y. *Chem. Phys. Lett.* **1999**, *314*, 141–151.

(109) Humphrey, W.; Dalke, A.; Schulten, K. *J. Mol. Graphics* **1996**, *14*, 33–8, 27−8.

(110) Kumar, S.; Payne, P. W.; Vásquez, M. *J. Comput. Chem.* **1995**, *17*, 1269–1275.

(111) Park, S.; Khalili-Araghi, F.; Tajkhorshid, E.; Schulten, K. *J. Chem. Phys.* **2003**, *119*, 3559–3566.

(112) Minh, D. D. L.; McCammon, J. A. *J. Phys. Chem. B* **2008**, *112*, 5892–5897.

(113) Forney, M. W.; Janosi, L.; Kosztin, I. *Phys. Rev. E* **2008**, *78*, 051913.

(114) Laio, A.; Rodriguez-Fortea, A.; Gervasio, F. L.; Ceccarelli, M.; Parrinello, M. *J. Phys. Chem. B* **2005**, *109*, 6714–6721.

(115) Bussi, G.; Laio, A.; Parrinello, M. *Phys. Rev. Lett.* **2006**, *96*, 090601.

(116) Lelièvre, T.; Rousset, M.; Stoltz, G. *J. Chem. Phys.* **2007**, *126*, 134111.

CT9004432